

Millimeter Wave Communications with an Intelligent Reflector: Performance Optimization and Distributional Reinforcement Learning

Qianqian Zhang¹, Walid Saad¹, and Mehdi Bennis²

¹Bradley Department of Electrical and Computer Engineering, Virginia Tech, VA, USA, Emails: {qqz93,walids}@vt.edu.

²Center for Wireless Communications, University of Oulu, Finland, Email: mehdi.bennis@oulu.fi.

Abstract

In this paper, a novel framework is proposed to optimize the downlink multi-user communication of a millimeter wave base station, which is assisted by a reconfigurable intelligent reflector (IR). In particular, a channel estimation approach is developed to measure the channel state information (CSI) in real-time. First, for a perfect CSI scenario, the optimal precoding transmission and power allocation is derived so as to maximize the sum of downlink rates towards multiple users, followed by the optimization of IR reflection coefficient to enhance the upper bound of the downlink transmission. Next, in the imperfect CSI scenario, a distributional reinforcement learning (DRL) approach is proposed to learn the optimal IR reflection and maximize the expectation of downlink capacity. In order to model the transmission rate's probability distribution, a learning algorithm, based on quantile regression (QR), is developed, and the proposed QR-DRL method is proved to converge to a stable distribution of downlink transmission rate. Simulation results show that, in the error-free CSI scenario, the proposed transmission approach yields over 20% and 2-fold increase in the downlink sum-rate, compared with a fixed IR reflection scheme and direct transmission scheme, respectively. Simulation results also show that by increasing the number of IR components, the downlink rate can be improved faster than by increasing the number of antennas at the BS. Furthermore, under limited knowledge of CSI, simulation results show that the proposed QR-DRL method, which learns a full distribution of the downlink rate, yields a better prediction accuracy and improves the downlink rate by 10% for online deployments, compared with a Q-learning baseline.

Index Terms – intelligent reflector; reinforcement learning; multi-user MISO; millimeter wave; beyond 5G.

I. INTRODUCTION

Next-generation cellular systems will inevitably rely on high-frequency millimeter wave (mmW) communications in order to meet the growing need for wireless capacity [1]. By leveraging

the large bandwidth at mmW frequencies, a wireless network can potentially deliver high-speed wireless links and meet stringent quality-of-service requirements. Moreover, the mmW band allows the implementation of small-sized antenna arrays and facilitates the use of massive multiple-input-multiple-output (MIMO) techniques to improve the wireless capacity. However, the high power cost and sophisticated signal processing of MIMO communications hinder the deployment of mmW frequencies into wide-scale commercial uses. Meanwhile, the high susceptibility to blockage caused by common objects, such as foliage and human bodies, yields the uncertainty of mmW channels [2]. Therefore, enabling reliable mmW links under blockage is a prominent challenge.

To overcome these intrinsic drawbacks of mmW, signal reflectors have been recently proposed to bypass obstacles and prolong the communication range [3]. By using reflectors, a non-line-of-sight (NLOS) mmW link can be compensated by creating multiple, connected line-of-sight (LOS) links [4]. Different from conventional relay stations (RSs) that receive, amplify (or decode), and forward the mmW signal, a reflector only reflects the incident signal towards the receiver, by inducing a phase shift. Therefore, the use of reflectors incurs no additional receiving noise or processing delay. Due to the nature of reflective surfaces, connected LOS links that pass through one or more reflectors can share the same frequency band, thus improving spectrum efficiency. In order to intelligently reflect incident signals with different phase shifts, a reconfigurable reflector can change the impedance of its antenna. By jointly adjusting the phase shifts of a large number of such low-cost semi-passive elements, an intelligent reflector (IR) can focus the reflected signal into a sharp beam, hence maximizing the beamforming performance gain with little energy cost [5]. Indeed, it has been shown in [6] that the use of reflectors is more appropriate for mmW networks than traditional RSs, in terms of energy, cost, and spectrum efficiency. However, performing optimal reflection on the IR requires precise channel state information (CSI). Due to the possible mobility of the served user equipment (UE) and the blockage-prone nature of mmW signals, it is difficult for a practical IR-assisted wireless network to continuously obtain an accurate value for CSI. Thus, to enable a real-time and efficient IR-aided transmission via mmW, the challenges of CSI estimation and network performance optimization under imperfect CSI must be properly addressed.

A. Related works

The use of IRs to enhance the performance of cellular networks has attracted significant recent attention in [4], [3], and [7]–[14]. In our previous work [4], we studied the deployment of a UAV-carried IR whose goal is to optimize the downlink mmW transmission towards a mobile outdoor user, using a deep learning. In [3], the design of a passive reflector and the estimation of the reflection gain are presented for urban mmW communications. The authors in [7] investigated the potential of a large intelligent surface for positioning, and the work in [8] studied the energy efficiency of reflector-assisted downlink communications. The authors in [9] jointly optimized the transmit beamforming from an access point and the reflective beamforming in IR to maximize the received UE signal power. The work in [10] proposed a hybrid MIMO framework that applies reflective arrays and conventional transmit antennas to improve mmW energy efficiency. However, the prior work on mmW reflectors in [3] focuses mainly on experimental measurements, while the IR-related works in [7]–[10] assumed perfect downlink CSI, which is challenging to know a priori in a practical network operation.

To obtain a precise value for CSI, recent works [11]–[14] have studied new approaches to efficiently measure CSI for IR-assisted communications. The authors in [11] proposed an asymptotic analysis of the uplink data rate for a large intelligent surface system with channel estimation error. In [12] and [13], a number of channel estimation protocols were investigated for reflecting beam training in a large intelligent surface communication system, based on deep learning and minimum mean squared error techniques, respectively. In order to reduce the overhead of channel estimation, authors in [14] aggregated adjacent reflective elements and measure the combined CSI for each group of IR components. However, none of these prior works in [11]–[14] studied the problem of IR-assisted cellular communications over mmW spectrum, which is more sensitive to the real-time CSI, due to its shorter wavelength and susceptibility to blockage.

B. Contributions

The main contribution of this paper is a novel framework for optimizing the IR-aided downlink transmission of a BS over mmW links. In particular, we propose a practical approach to estimate the downlink CSI, such that the reflection coefficient of the IR can be optimized in a real-time manner so as to maximize the downlink capacity of multiple UEs. Our main contributions are:

- We derive the optimal precoding transmission and power allocation, under the assumption of perfect CSI, and optimize the reflection coefficient of the IR to further enhance the upper bound of the downlink rate.
- Given that receivers' noise induces errors to the measured CSI, we study the optimization of the IR-aided transmission with imperfect CSI. In particular, we propose a distributional reinforcement learning (DRL) approach to model the distribution function of the downlink rate, and, then, the IR reflection coefficient is optimized to maximize the expected downlink capacity. To model the rate's probability distribution, an iterative learning algorithm based on quantile regression (QR) is developed, so that the optimal reflection coefficient of the IR is learned based on UEs' feedback. We analytically prove that the proposed QR-DRL approach converges to a stable distribution of IR-aided downlink transmission rates.
- For a scenario with error-free CSI, simulation results first show that, the proposed transmission approach outperforms two baselines: (i) a fixed IR reflection and (ii) a direct transmission scheme. As the BS transmit power increases from 20 to 40 dBm, the proposed method yields over 30% and 3-fold increases in the average downlink sum-rate, compared with both baselines. Meanwhile, the proposed approach shows over 20% and 2-fold increase in performance, as the downlink bandwidth increases from 0.1 to 3 MHz. When the number of transmit antennas increases from 4 to 49, the average sum-rates resulting from the three methods increase, and the proposed method improves the downlink sum-rate by over 20%, compared with the fixed reflection scheme. As the number of IR components increases, the performance of the direct transmission scheme remains the same, while the proposed method and the direct transmission approach yield higher rates. Compared with the fixed reflection scheme, the proposed method improves the transmission performance by over 35%. Moreover, simulation results show that deploying more IR components is more efficient to increase the average downlink rate, compared with more antennas at the BS.
- For a scenario with imperfect CSI, simulation results show that the QR-DRL method, which learns a full distribution of the downlink sum-rate, has a slower convergence rate, but yields a better prediction accuracy and improves the average spectrum efficiency by over 10% for online deployments, compared with a Q-learning baseline.

The rest of this paper is organized as follows. Section II presents the system model. The transmission and reflection under perfect CSI is optimized in Section III. In Section IV, the

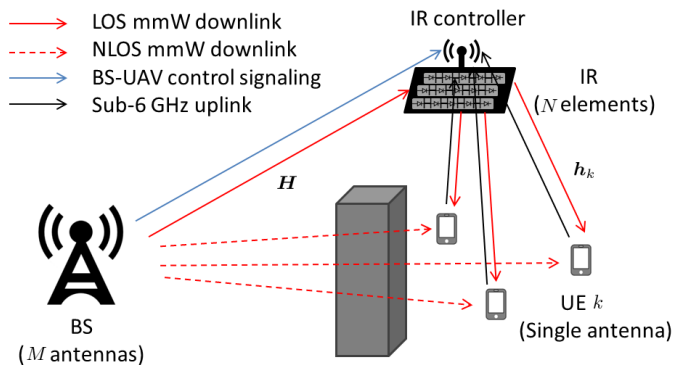


Fig. 1: The multi-user downlink communications from a multi-antennas BS, reflected via an IR, to a group of NLOS UEs, over mmW links.

downlink sum-rate is maximized under limited knowledge of CSI, where a learning framework is proposed to tackle the uncertainty of downlink CSI and optimize the reflection downlink capacity. Simulation results are presented in Section V and conclusions are drawn in Section VI.

Notation: Italic letters a and A are both scalar, the bold letter \mathbf{a} is a vector, the bold capital \mathbf{A} is a matrix, and $a_{i,j}$ is the element on the i -th row and the j -th column of \mathbf{A} . The calligraphic capital \mathcal{A} denotes a set. The blackboard bold \mathbb{R} , \mathbb{C} and \mathbb{N}^+ are the sets of real numbers, complex numbers, and positive integer numbers, respectively. $\mathcal{CN}(\boldsymbol{\mu}, \boldsymbol{\Sigma})$ denotes a complex normal random variable with mean vector $\boldsymbol{\mu}$ and covariance matrix $\boldsymbol{\Sigma}$. $\|\mathbf{A}\|_F$ is the Frobenius norm of the matrix \mathbf{A} , and $\text{tr}(\mathbf{A})$ denotes the trace. $\|\mathbf{a}\|$ is the two-norm of a vector. $|a|$, $\angle a$, and $\text{Re}\{a\}$ are the absolute value, angle and real part of the complex number in polar coordinates. $(\cdot)^T$, $(\cdot)^H$, $(\cdot)^{-1}$, and $(\cdot)^+$ are transport, Hermitian (conjugate transport), inverse, and pseudo-inverse, respectively. \inf and \sup are the infimum and supremum of a set. $\text{diag}(\mathbf{a})$ is a diagonal matrix with the entries of \mathbf{a} on its diagonal. $\mathbb{1}_{a=0}$ denotes an indicator function that equals to 1 if “ $a = 0$ ” is true, $\mathbf{1}_n$ is an $n \times 1$ all-ones vector, and \mathbf{I}_n is the $n \times n$ identify matrix.

II. SYSTEM MODEL

Consider a cellular base station (BS) that transmits over the mmW frequency band to provide downlink wireless communication to a group of outdoor users, and let \mathcal{K} be the set of K users. We assume that the served users are located within a hotspot area, and each UE is equipped with a single antenna. In order to compensate for the fast attenuation of mmW signals, the BS is equipped with $M \in \mathbb{N}^+$ directional antenna arrays for beamforming. Therefore, in a LOS case, downlink communication can be reliable and efficient. However, due to the need for transmission

over long distances, the BS-UE link can be blocked by common objects, such as buildings and foliage, which can seriously attenuate mmW signals. In particular, within a hotspot area, the density of UEs is usually high, and the body of the human user becomes a main blockage source. Therefore, as done in [8] and [15], we assume that the direct link from the BS to each hotspot UE is always NLOS, and, thus, the received signal via the direct link is negligible.

To overcome mmW blockage and improve the received UE power, an IR can be deployed to assist the mmW downlink transmission. As shown in Fig. 1, an IR can potentially replace one direct NLOS link with two connected LOS links, by reflecting the mmW signals from the BS towards each served UE. We assume that the IR consists of $N \in \mathbb{N}^+$ reflective components. By controlling the biasing voltage to vary the impedance of the antenna, the reflection coefficient of each IR element can be dynamically adjusted. As such, the mismatch between the antenna impedance and the carrier wave will reflect a portion of the incident signal [16]. Note that an IR is a passive device, which cannot sense any CSI or process received signals. To enable information exchange, an active antenna must be embedded onto the IR controller to receive control signal from the BS and feedback information from served UEs. As shown in Fig. 1, the BS assigns a specific channel to the IR for control signaling. Meanwhile, the UE's feedback can be obtained via the uplink. Note that, this active antenna at the IR controller only receives and processes signals for control purposes, while downlink communication signals are transferred through the reflection component at the IR.

A. Communication model

Our system can be viewed as a multi-user multiple-input-single-output (MISO) communication model, in which the BS serves downlink UEs via a common frequency band, while being assisted by an IR [8]. The discrete-time complex baseband channel of the BS-IR link is denoted by $\mathbf{H} \in \mathbb{C}^{N \times M}$, and the channel from the IR to UE $k \in \mathcal{K}$ is $\mathbf{h}_k \in \mathbb{C}^{1 \times N}$. In order to provide downlink communications to multiple UEs, the BS precodes the transmit signal as an $M \times 1$ vector $\mathbf{s} = \sum_{k=1}^K \sqrt{p_k} \mathbf{w}_k \alpha_k$, where $\sqrt{p_k}$ is the transmit power, $\mathbf{w}_k \in \mathbb{C}^{M \times 1}$ is the precoding vector, and α_k is the unit-power complex-valued information symbol for UE k . Here, the power allocation is subject to a maximum power constraint P_{\max} of the BS, where $\|\mathbf{s}\|^2 = \sum_{k \in \mathcal{K}} p_k \|\mathbf{w}_k\|^2 \leq P_{\max}$.

We consider that all IR components are equally spaced in a two-dimensional plane to form the IR. Let \mathcal{N} be the index set of N IR elements. For each component $n \in \mathcal{N}$, we denote the phase shift of the reflection by $\theta_n \in [0, 2\pi)$ and the amplitude reflection coefficient by $a_n \in [0, 1]$.

Consequently, the IR's reflection coefficient will be given by $\Theta = \text{diag}(a_1 e^{j\theta_1}, \dots, a_N e^{j\theta_N})$.

Therefore, after the reflection, the received signal at UE k will be:

$$y_k = \mathbf{h}_k \Theta \mathbf{H} \mathbf{s} + z_k, \quad (1)$$

where $z_k \sim \mathcal{CN}(0, \sigma^2)$ is the receiver noise at UE k . Here, we note that the downlink channel of the BS-IR-UE link towards UE k can be equivalently expressed by

$$\mathbf{h}_k \Theta \mathbf{H} = \phi \mathbf{G}_k, \quad (2)$$

where $\phi = [a_1 e^{j\theta_1}, \dots, a_N e^{j\theta_N}] \in \mathbb{C}^{1 \times N}$ is a vector of the reflection coefficient and $\mathbf{G}_k = \text{diag}(\mathbf{h}_k) \mathbf{H} \in \mathbb{C}^{N \times M}$ is the CSI of the connected BS-IR-UE link towards UE k without any phase shift. This formulation separates the reflection coefficient ϕ from the propagation channel \mathbf{G}_k . For tractability, we assume that UEs' locations remain unchanged during one coherence time of the IR's transmission. Thus, the received signal of UE k can be rewritten as $y_k = \phi \mathbf{G}_k \mathbf{s} + z_k$. Therefore, the downlink signal-to-interference-and-noise ratio (SINR) from the BS, reflected by the IR, to each UE $k \in \mathcal{K}$ can be given by,

$$\eta_k(\mathbf{W}, \mathbf{p}, \phi) = \frac{p_k |\mathbf{h}_k \Theta \mathbf{H} \mathbf{w}_k|^2}{\sum_{i \neq k, i \in \mathcal{K}} p_i |\mathbf{h}_k \Theta \mathbf{H} \mathbf{w}_i|^2 + \sigma^2} = \frac{p_k |\phi \mathbf{G}_k \mathbf{w}_k|^2}{\sum_{i \neq k, i \in \mathcal{K}} p_i |\phi \mathbf{G}_k \mathbf{w}_i|^2 + \sigma^2}, \quad (3)$$

where $\mathbf{W} = [\mathbf{w}_1, \dots, \mathbf{w}_K] \in \mathbb{C}^{M \times K}$ is a linear precoding matrix, and $\mathbf{p} = [p_1, \dots, p_K] \in \mathbb{R}^K$ is the power allocation vector at the BS. The sum of achievable downlink rates that the IR-assisted communication can provide to the hotspots UE is

$$r(\mathbf{W}, \mathbf{p}, \phi) = \sum_{k=1}^K b \log_2 (1 + \eta_k(\mathbf{W}, \mathbf{p}, \phi)), \quad (4)$$

where b is the downlink bandwidth.

B. Channel Measurement

Considering the susceptibility of mmW signals to blockage, a simple body movement of the human user can substantially change the CSI of the BS-IR-UE link for each UE. Therefore, a real-time channel estimation is necessary to measure the accurate CSI value, so that the reflection coefficient can be optimally determined. Here, we let $\mathcal{G} = \{\mathbf{G}_k\}_{\forall k \in \mathcal{K}}$ be the set of CSI from the BS, reflected by the IR, towards all downlink UEs.

The CSI of a wireless link is assumed to be constant within each coherence time slot τ , where $\tau = \lambda_f / v_e$ is the ratio of the carrier wavelength λ_f to the UE's speed v_e . Since UEs in the

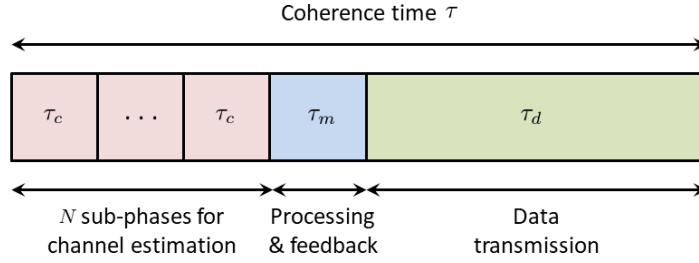


Fig. 2: One coherence time slot τ is divided into three sub-phases, where $\tau = N\tau_c + \tau_m + \tau_d$.

hotspot are often confined to geographically constrained spaces in which mobility is either rare or very low, the coherence time slot of the considered mmW communication can be considered to be long enough to enable real-time channel measurement. Given that the IR is a passive antenna array that cannot transmit or decode any signal, a time division duplex (TDD) approach is used whereby the BS-IR-UE channels are estimated, by exploiting the channel reciprocity, using the uplink pilot signals from UEs [13]. Therefore, within one channel coherence time slot, three sequential phases [14] are employed to measure the CSI: Uplink training phase, processing phase, and downlink transmission phase, as shown in Fig. 2.

Throughout the uplink training phase within a time duration $N\tau_c$, the UEs transmit mutually orthogonal pilot symbols s_k , where $|s_k|^2 = p_c$ is the transmit power of each UE, and an ON/OFF state control is applied to the IR. An IR element $n \in \mathcal{N}$ in the ON state will reflect the incident signal without any phase shift, in which case we have $a_n = 1$ and $\theta_n = 0$; while an IR element in the OFF state will capture the incident signals without any reflection, i.e., $a_n = 0$. Here, the uplink training phase is evenly divided into N sub-phases, and within each sub-phase τ_c , only one IR component is ON¹, while all the other IR components are OFF. Let $\mathbf{g}_{n,k} \in \mathbb{C}^{1 \times M}$ be the n -th row vector of the channel matrix \mathbf{G}_k . Then, the received training signal vector from the downlink UEs, reflected by the n -th IR element, to the BS can be expressed as $\mathbf{y}_n = \sum_{k=1}^K \mathbf{g}_{n,k}^H s_k + \mathbf{z}$, where $\mathbf{z} \sim \mathcal{CN}(\mathbf{0}, \sigma_{\text{BS}}^2 \mathbf{I}_M)$ is the noise vector at the BS. Once the uplink pilot phase is finished, the BS will receive N independent observation vectors $\{\mathbf{y}_n\}_{n=1, \dots, N}$. Then, based on the least-square estimation, which is known to be a minimum-variance unbiased estimator, the channel vector from the BS, reflected by the n -th IR component, to UE k can be calculated via

$$\hat{\mathbf{g}}_{n,k} = (\mathbf{y}_n s_k^{-1})^H \triangleq \mathbf{g}_{n,k} + \tilde{\mathbf{g}}_{n,k}, \quad (5)$$

where $\tilde{\mathbf{g}}_{n,k} = (\mathbf{z} s_k^{-1})^H$ is the uncorrelated channel estimation error, caused by the receiver noise at the BS. Therefore, the measurement results of the downlink channel matrix for each UE $k \in \mathcal{K}$

¹In the ON state, the energy loss of signal reflection will be counted in the measurement of CSI.

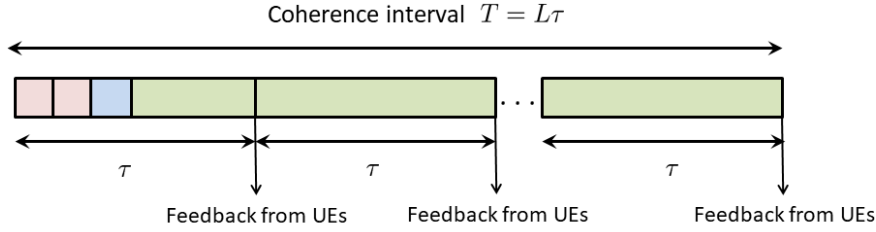


Fig. 3: Multiple time slots are grouped into a coherence interval $T = L\tau$, during which the channel measurement is employed only during the first τ , while all the following steps are used for data transmission.

can be denoted by $\hat{\mathbf{G}}_k = [\hat{\mathbf{g}}_{1,k}^T, \dots, \hat{\mathbf{g}}_{N,k}^T]^T \in \mathbb{C}^{N \times M}$. At the end of the signal processing phases, the BS will send the channel estimation result $\hat{\mathbf{G}} = \{\hat{\mathbf{G}}_k\}_{\forall k \in \mathcal{K}}$ to the IR, via the control channel. Once the processing phase is finished, the transmission phase τ_d will start, during which the IR will provide the downlink service towards UEs, while optimizing the reflection coefficient to maximize the downlink rate in (4).

However, the theoretical upper-bound of the transmission rate in (4) is difficult to achieve in practice. This is because the optimization of the reflection coefficient ϕ is based on the estimated CSI $\{\hat{\mathbf{G}}_k\}_{k=1, \dots, K}$, which is subject to measurement errors. Here, the mean square error (MSE) of the channel estimation for each BS-IR-UE MISO channel can be defined as

$$\mathbb{E} \left\{ \|\hat{\mathbf{G}}_k - \mathbf{G}_k\|_F^2 \right\} = \mathbb{E} \left\{ \sum_{n=1}^N \|\tilde{\mathbf{g}}_{n,k}\|^2 \right\} = \sum_{n=1}^N \mathbb{E} \left\{ \frac{\|z\|^2}{p_c} \right\} = \frac{NM\sigma_{BS}^2}{p_c}. \quad (6)$$

Given that the uplink power p_c of each UE is strictly limited, as the numbers of BS antennas M and IR elements N increase, the MSE of the estimated CSI will become larger. In order to guarantee an efficient reflection transmission, it is necessary to optimize the IR coefficient, using the feedback from downlink UEs. Hence, beyond the pilot-aided training at the beginning of the time slot, more information about CSI can be acquired from UEs' feedback during the following transmission phase to improve downlink performance, as detailed in Section IV.

Furthermore, we note that as the number of IR elements N becomes larger, the downlink communication duration $\tau_d = \tau - N\tau_c - \tau_m$ will be too short for efficient downlink service. To reduce the average time for uplink training, we group multiple time slots to form a longer coherence interval $T = L\tau$, where $L \in \mathbb{N}^+$, such that the channel measurement is employed only at the beginning of the first time slot τ , while all remaining time steps are used for downlink communication, as shown in Fig. 3. This framework is supported by the experimental results in [17], where the mmW channel was shown to exhibit a slower change as the beamwidth of directional transmissions narrows. Therefore, with beamforming transmission, the downlink CSI

within multiple coherent times can be considered as a constant, and it is possible to consider the IR transmission over a long interval T .

In consequence, the total amount of downlink data that the IR-aided transmission provides to the hotspot UEs within one coherence interval T is

$$R(\mathbf{W}, \mathbf{p}, \phi | \hat{\mathcal{G}}) = \sum_{l=1}^L t_l \cdot r_l(\mathbf{W}, \mathbf{p}, \phi | \hat{\mathcal{G}}), \quad (7)$$

where t_l and r_l are the transmission duration and the downlink sum-rate at the l -th time slot. Based on Fig. 3, we have $t_l = \tau_d$ for $l = 1$ and $t_l = \tau$ for $l = 2, \dots, L$. Meanwhile, if the values of \mathbf{W} , \mathbf{p} , and ϕ keeps the same for all $l = 1, \dots, L$, then $r_l = r$ and $R = (T - N\tau_c - \tau_m) \cdot r \triangleq T_d \cdot r$, where $T_d = T - N\tau_c - \tau_m$ is the efficient transmission time during one coherence interval.

C. Problem Formulation

Our goal is to optimize the downlink transmission to a group of UEs by intelligently adjusting the reflection coefficients, such that the total downlink transmission within a coherence interval is maximized, i.e.,

$$\max_{\mathbf{W}, \mathbf{p}, \phi} R(\mathbf{W}, \mathbf{p}, \phi | \hat{\mathcal{G}}) \quad (8a)$$

$$\text{s. t.} \quad \text{tr}(\mathbf{W}\mathbf{P}\mathbf{W}^H) \leq P_{\max}, \quad (8b)$$

$$|\phi_n| \leq 1, \forall n \in \mathcal{N}, \quad (8c)$$

where $\mathbf{P} = \text{diag}(\mathbf{p}) = \text{diag}(p_1, \dots, p_K)$. The objective function in (8a) is the amount of transmitted downlink data within one T . (8b) limits the maximum transmit power at the BS, and (8c) is the constraint on the IR's parameters. Here, the values of the precoding matrix \mathbf{W} and the power allocation \mathbf{p} are controlled by the BS, and the reflection coefficient ϕ is a variable controlled by the IR.

Note that, this problem is challenging and differs from prior works [7]–[10] on IRs. First, given the non-convex objective function (8a) with respect to \mathbf{W} , \mathbf{p} , and ϕ , the optimization problem (8) is difficult to solve. Second, since the IR is a passive element that cannot transmit or process signals, channel measurements must rely on pilot signals, transmitted from downlink UEs towards the BS. Hence, the measurement result $\hat{\mathbf{G}}_k$ is the effective channel matrix of the connected BS-IR-UE link for each UE k , instead of the separated CSI of \mathbf{H} for the BS-IR link and \mathbf{h}_k for the IR-UE link, as shown in [7]–[10]. Moreover, communication over mmW frequencies requires a higher CSI accuracy. Unfortunately, uplink pilot training is subject to measurement errors,

which renders the IR-aided transmission less reliable. In order to address the aforementioned challenges, a learning-based approach can be applied to capture the uncertainty of the downlink channel and enable the efficient transmission via the IR, under imperfect CSI.

Before exploring the learning algorithm (in Section IV), in Section III, we first analyze a simple case in which the estimated CSI is error-free. In this case, the beamforming transmission at the BS and the reflection coefficient of the IR will be optimized, under perfect CSI. Next, in Section IV, the reflection optimization with the limited knowledge of CSI will be studied.

III. OPTIMAL TRANSMISSION AND REFLECTION WITH PERFECT CSI

In this section, we optimize the beamforming transmission at the BS and the reflection coefficient at the IR, respectively, to maximize the sum of downlink transmission in (7), under the assumption of perfect CSI.

A. Optimal transmission at BS with perfect CSI

During each coherence interval, the BS can optimize the precoder matrix \mathbf{W} and the power allocation \mathbf{p} , given an accurate CSI $\hat{\mathcal{G}} = \mathcal{G}$ and a fixed reflection coefficient ϕ of the IR, i.e.

$$\max_{\mathbf{W}, \mathbf{p}} R(\mathbf{W}, \mathbf{p} | \mathcal{G}, \phi) = T_d \cdot r(\mathbf{W}, \mathbf{p} | \mathcal{G}, \phi) \quad (9a)$$

$$\text{s. t.} \quad \text{tr}(\mathbf{W} \mathbf{P} \mathbf{W}^H) \leq P_{\max}. \quad (9b)$$

Given the non-convex objective function (9a) with respect to \mathbf{W} and \mathbf{p} , the optimization problem (9) is very challenging to solve. In order to simplify the analysis, the BS can employ zero-forcing (ZF) transmission for interference mitigation, which is known to be optimal in the high-SINR regime [18]. In order to achieve a perfect interference suppression, as done in [8] and [19], we assume that $M \geq K$, which means the number of transmit antennas M is greater than or equal to the number of served UEs K . Let $\mathbf{J}_\phi = [(\phi \mathbf{G}_1)^T, \dots, (\phi \mathbf{G}_K)^T]^T \in \mathbb{C}^{K \times M}$ be the downlink channel matrix from the BS, reflected by the IR with coefficient ϕ , to the UEs. Then, with the assumption of perfect CSI, the ZF precoder is given by $\mathbf{W} = \mathbf{J}_\phi^+$, and the optimization problem (9) becomes

$$\max_{\mathbf{p}} \sum_{k=1}^K \log_2 \left(1 + \frac{p_k}{\sigma^2} \right) \quad (10a)$$

$$\text{s. t.} \quad \text{tr}(\mathbf{J}_\phi^+ \mathbf{P} (\mathbf{J}_\phi^+)^H) = P_{\max}. \quad (10b)$$

Given the concave objective function (10a) and the linear constraint (10b) with respect to \mathbf{p} , a closed-form expression for the optimal power allocation can be given, based on water-filling algorithm, as follows:

Proposition 1. *Under a perfectly-known CSI and a ZF precoder $\mathbf{W} = \mathbf{J}_\phi^+$, the optimal power allocation \mathbf{p}^* that maximizes the sum of downlink rates in (10a) is $p_k^* = \frac{1}{Ku_k}[\sigma^2(\sum_{i=1}^K u_i - Ku_k) + P_{\max}]$, where $u_k = \sum_{j=1}^M |w_{j,k}|^2$, $\forall k \in \mathcal{K}$.*

Proof. Constraint (10b) can be rewritten as $P_{\max} = \text{tr}(\mathbf{W}\mathbf{P}\mathbf{W}^H) = \text{tr}(\mathbf{W}\mathbf{P}^{1/2}(\mathbf{P}^{1/2}\mathbf{W})^H) = \|\mathbf{W}\mathbf{P}^{1/2}\|_F^2 = \sum_{k=1}^K \sum_{j=1}^M |w_{j,k}|^2 p_k = \sum_{k=1}^K u_k p_k$. Then, the Lagrangian function of the optimization problem (10) can be given by $\mathcal{L}(\mathbf{p}, \lambda) = \sum_{k \in \mathcal{K}} \log_2(1 + p_k/\sigma^2) - \lambda(\sum_{k=1}^K u_k p_k - P_{\max})$. Based on the Karush–Kuhn–Tucker conditions, we have: (1) $\nabla_{p_k} \mathcal{L}(\mathbf{p}, \lambda) = 0, \forall k$, (2) $\sum_{k=1}^K u_k p_k = P_{\max}$. By solving the equation set, we find $p_k^* = \frac{1}{\ln 2} \frac{1}{u_k \lambda^*} - \sigma^2, \forall k$, and $\lambda^* = \frac{K}{\ln 2(P_{\max} + \sigma^2 \sum_{i=1}^K u_i)}$. Therefore, the optimal power allocation is $p_k^* = \frac{P_{\max} + \sigma^2 \sum_{i=1}^K u_i}{Ku_k} - \sigma^2, \forall k$. \square

Therefore, with the ZF precoder $\mathbf{W}^* = \mathbf{J}_\phi^+$ and the optimal power allocation \mathbf{p}^* in Proposition 1, the downlink transmission is optimized at the BS side. Once (9) is solved, the BS will send \mathbf{W}^* and \mathbf{p}^* to the IR via the control channel. Moreover, during the following communication stage, the values of \mathbf{W}^* and \mathbf{p}^* will remain fixed.

B. Optimal reflection at IR with perfect CSI

Given the precoding \mathbf{W}^* and power allocation \mathbf{p}^* at the BS side, the IR can further improve the downlink transmission by optimizing its reflection parameter ϕ , i.e.,

$$\max_{\phi} R(\phi|\mathcal{G}, \mathbf{W}^*, \mathbf{p}^*) = T_d \cdot r(\phi|\mathcal{G}, \mathbf{W}^*, \mathbf{p}^*) \quad (11a)$$

$$\text{s. t. } |\phi_n| \leq 1, \forall n \in \mathcal{N}, \quad (11b)$$

where the objective function (11a) is the amount of transmitted downlink data within one coherence interval, and (11b) is the constraint on the IR's parameters. Note that (11a) is a non-convex function with respect to the reflection coefficient ϕ . Therefore, the optimization problem (11) is very challenging to solve.

In order to simplify the analysis, instead of maximizing the downlink capacity directly, we maximize the upper bound of (11a). Based on the Jensen's inequality, we have [20]

$$r(\phi) = \sum_{k=1}^K \log_2(1 + \eta_k(\phi)) \leq K \log_2 \left(1 + \frac{1}{K} \sum_{k=1}^K \eta_k(\phi) \right). \quad (12)$$

Therefore, the optimization problem to maximize the upper bound of the downlink transmission can be given by

$$\max_{\phi} \sum_{k=1}^K \eta_k(\phi) = \sum_{k=1}^K \frac{|\phi \mathbf{G}_k \tilde{\mathbf{w}}_k^*|^2}{\sum_{i \neq k, i \in \mathcal{K}} |\phi \mathbf{G}_k \tilde{\mathbf{w}}_i^*|^2 + \sigma^2} \quad (13a)$$

$$\text{s. t. } |\phi_n| \leq 1, \forall n \in \mathcal{N}, \quad (13b)$$

where $\tilde{\mathbf{w}}_k^* = \sqrt{p_k^*} \mathbf{w}_k^*$ for each $k \in \mathcal{K}$. Given that (13) is a multiple-ratio fractional programming problem, we can transfer it into the following form [21, Theorem 2]:

$$\max_{\phi, \lambda} f(\phi, \lambda) = \sum_{k=1}^K 2\text{Re}\{\lambda_k^H \phi \mathbf{G}_k \tilde{\mathbf{w}}_k^*\} - \sum_{k=1}^K |\lambda_k|^2 \left(\sum_{i \neq k, i \in \mathcal{K}} |\phi \mathbf{G}_k \tilde{\mathbf{w}}_i^*|^2 + \sigma^2 \right) \quad (14a)$$

$$\text{s. t. } |\phi_n| \leq 1, \forall n \in \mathcal{N}, \quad (14b)$$

where $\lambda = [\lambda_1, \dots, \lambda_K]^T$ is the auxiliary variable vector. In order to solve (14), an iterative approach will be applied to optimize ϕ and λ alternatively. First, for a given ϕ , the optimal value of λ_k can be obtained by setting $\frac{\partial f}{\partial \lambda_k} = 2\phi \mathbf{G}_k \tilde{\mathbf{w}}_k^* - 2\lambda_k (\sum_{i \neq k} |\phi \mathbf{G}_k \tilde{\mathbf{w}}_i^*|^2 + \sigma^2) = 0$, i.e.

$$\lambda_k^0 = \frac{\phi \mathbf{G}_k \tilde{\mathbf{w}}_k^*}{\sum_{i \neq k} |\phi \mathbf{G}_k \tilde{\mathbf{w}}_i^*|^2 + \sigma^2}. \quad (15)$$

Second, given a fixed λ , the optimal value ϕ can be obtained by solving the following problem,

$$\max_{\phi} f(\phi) = -\phi \mathbf{U} \phi^H + 2\text{Re}\{\phi \mathbf{v}\} - C \quad (16a)$$

$$\text{s. t. } |\phi_n| \leq 1, \forall n \in \mathcal{N}, \quad (16b)$$

where the matrix $\mathbf{U} = \sum_{k=1}^K |\lambda_k|^2 \sum_{i \neq k} \mathbf{G}_k \tilde{\mathbf{w}}_i^* \tilde{\mathbf{w}}_i^{*H} \mathbf{G}_k^H$, the vector $\mathbf{v} = \sum_{k=1}^K \lambda_k^H \mathbf{G}_k \tilde{\mathbf{w}}_k^*$, and the constant $C = \sum_{k=1}^K |\lambda_k|^2 \sigma^2$. Given that \mathbf{U} is positive-definite, f is quadratic concave with respect to ϕ . Meanwhile, the constrain (16b) is a convex set, so the optimization problem (16) is solvable using conventional gradient-based method [22]. In consequence, the optimal reflection coefficient ϕ can be determined using an iterative approach, which is summarized in Algorithm 1. Here, we note that f is a convex function with respect to each ϕ_k and λ_n . Therefore, Algorithm 1 is guaranteed to converge to the global optimum.

In consequence, the optimal beamforming transmission of the BS and the optimal reflection of the IR to maximize the downlink rate are given in Proposition 1 and Algorithm 1. However, we stress that Proposition 1 and Algorithm 1 have been derived under the assumption of perfect CSI. However, in presence of channel estimation errors, Algorithm 1 cannot guarantee an efficient downlink transmission. Therefore, under limited CSI, it is necessary for the IR to optimize the reflection parameter coefficient ϕ , based on the feedback of downlink UEs.

Algorithm 1 Optimal IR coefficient with perfect CSI

Initialize the reflection coefficient $\phi = \mathbf{I}_N$, the precoding matrix $\mathbf{W}^* = \mathbf{J}_\phi^+$, and the power allocation \mathbf{p}^* based on Proposition 1.

Repeat

1. Update λ by (15);
2. Update ϕ by solving (16) using gradient-based convex optimization method;

Until convergence.

IV. OPTIMAL REFLECTION WITH LIMITED CSI

In this section, the reflection optimization of the IR is studied, considering the estimation error in the measured CSI $\hat{\mathcal{G}}$, while Algorithm 1 is used as initialization for the IR-aided transmission.

A. Problem formulation

In order to evaluate the downlink performance, each UE k can update its received signal to the IR controller, via the uplink channel, at the end of each time slot. Let $\mathbf{y}_l = [y_{l,1}, \dots, y_{l,K}] \in \mathbb{C}^{1 \times K}$ be the received signal vector of downlink UEs during the l -th time slot, where $y_{l,k} = \phi_l \mathbf{G}_{l,k}(\mathbf{x})\mathbf{s} + z_k$, and $\phi_l = [\phi_{l,1}, \dots, \phi_{l,N}]$ is the reflection coefficient of the IR. If the received signal power $|y_{l,k}|^2$ for each UE k is small, then the optimal reflection from Algorithm 1 is actually not reliable, due to the channel estimation error. In this case, the IR controller can compare the actual received signal $y_{l,k}$ with the expected received signal $\hat{y}_{l,k} = \phi_l \hat{\mathbf{G}}_k \mathbf{s}$, which is calculated via the measured CSI. Then, the signal deviation at the receiver will be obtained by $e_{l,k} = y_{l,k} - \hat{y}_{l,k} = \phi_l (\mathbf{G}_k - \hat{\mathbf{G}}_k) \mathbf{s} + z_k$, where the value of downlink channel \mathbf{G}_k is fixed but unknown to the IR. Let $\mathbf{e}_l = [e_{l,1}, \dots, e_{l,K}] \in \mathbb{C}^{1 \times K}$ be the deviation vector of the l -th time slot, and $\Delta\Theta = \text{diag}(\Delta\theta_1, \dots, \Delta\theta_N) \in \mathbb{C}^{N \times N}$ be an *action* matrix that shifts the phase of the reflection parameter ϕ via $\phi \times \Delta\Theta$, while keeping the reflection amplitude the same.

Consequently, the IR controller with limited CSI can improve the reflection parameter via $\phi_l \times \Delta\Theta$, at the end of each slot $l = 1, \dots, L-1$, in order to maximize the total amount of downlink data from the next time slot $l+1$ to the end of the coherence interval $l=L$, i.e.

$$\max_{\Delta\Theta} \sum_{t=l+1}^L \tau \cdot r_t(\phi_l \times \Delta\Theta | \mathbf{e}_l, \mathbf{y}_l, \hat{\mathcal{G}}, \mathbf{W}^*, \mathbf{p}^*) \quad (17a)$$

$$\text{s. t. } |\Delta\theta_n| = 1, \forall n \in \mathcal{N}. \quad (17b)$$

The process of the IR-aided transmissions under imperfect CSI is summarized in Algorithm 2. Meanwhile, since the values of \mathbf{W}^* and \mathbf{p}^* remain the same during the transmission phase, we will omit them in the following discussion.

Algorithm 2 Reflection optimization of the IR under imperfect CSI

1. **Uplink training phase:** the downlink CSI $\hat{\mathcal{G}}$ is estimated as elaborated in Section II-B;
 2. **Processing phase:**
 - A. BS optimizes the precoding matrix \mathbf{W}^* and the power allocation \mathbf{p}^* , according to Proposition 1;
 - B. The IR optimizes the reflection parameter ϕ^* , based on Algorithm 1;
 3. **Transmission phase:** At the end of each time slot $l = 1, \dots, L - 1$,
 - A. Each UE k updates its received signal $y_{l,k}$ via uplink;
 - B. The IR calculates the deviation vector e_l , and optimizes the reflection parameter ϕ in (17), based on Algorithm 3 in Section IV-C.
-

However, the optimization problem in (17) is very challenging to solve. For each UE k , the feedback $y_{l,k}$ and signal deviation $e_{l,k}$ during each time slot are both scalar, and, thus, they cannot provide sufficient information for the IR to reconstruct the channel matrix \mathbf{G}_k which has $N \times M$ scalar elements. Meanwhile, due to the receiver's noise, it is impossible to have a perfect CSI via uplink training phase. One traditional approach to cancel the effect of noise is to average the estimation results from multiple measurements. However, repeated measurements will consume significant time and power, which is impractical in the considered problem. In order to solve the problem of CSI estimation, a reinforcement learning (RL) framework is introduced to improve the reflection parameter of the IR during the service of downlink transmission. In the RL design, the BS and IR are not required to have perfect measurement on the CSI or have an explicit knowledge of channel statistics. By observing the UEs' feedback during each time slot, the proposed algorithm can automatically acquire the real-time downlink statistics. Moreover, an offline process can be applied to train the RL model, such that the online optimization of the IR reflection can be done in a real-time and efficient manner.

B. Reinforcement learning

As shown in Fig. 4, in our RL framework, the connected channels $\{\phi \mathbf{G}_k\}_{\forall k}$ represent the *environment* of downlink communications, the deviation vector e is defined as the *state*, which evaluates the accuracy of the measured downlink CSI $\{\hat{\mathbf{G}}_k\}_{\forall k}$, and the IR controller is called the *agent* which learns the optimal reflection coefficient ϕ from the feedback of downlink UEs. In order to model the agent-environment interactions, a Markov decision process (MDP) model $(\mathcal{E}, \mathcal{A}, r, P, \gamma)$ is used, where \mathcal{E} is the space of all possible states e , and $\mathcal{A} = \{\Delta\Theta | \forall n, |\Delta\theta_n| = 1\}$ is the space of actions, r is the reward function, which is defined as the downlink sum-rate towards all UEs during a time slot, $P(e' | e, \Delta\Theta)$ is the transition probability of the state from e to e' after taking action $\Delta\Theta$, and $\gamma \in (0, 1)$ is the discount factor.

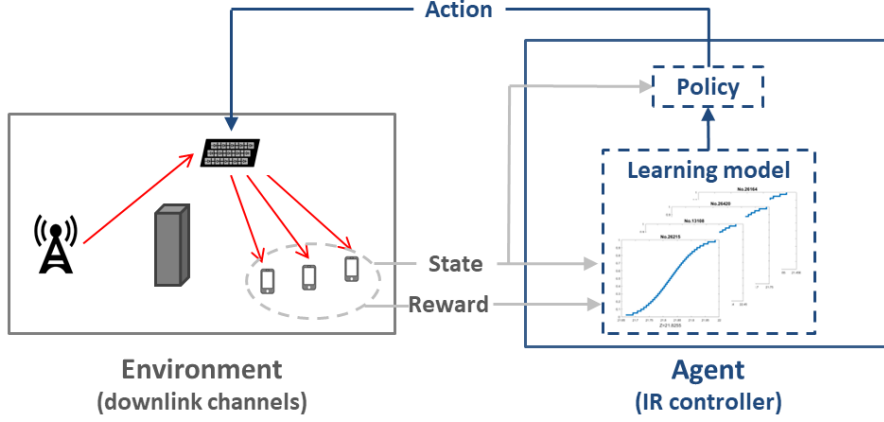


Fig. 4: An illustration of the RL framework for learning and optimizing the IR-aided downlink transmissions.

After observing a deviation vector e_l , the IR aims to adjust its reflection coefficient to accommodate the actual downlink CSI via $\phi_{l+1} = \phi_l \times \Delta\Theta$, such that the sum of future data rate r_t for the following time slot $t = l + 1, \dots, L$ can be maximized. In order to quantify the potential of each action matrix $\Delta\Theta$ to improve the future reward, first, a *policy* $\pi(\Delta\Theta|e)$ is defined as a probability over each action $\Delta\Theta \in \mathcal{A}$, conditioned on each state $e \in \mathcal{E}$. Then, for each stationary policy π , the potential of each state-action pair $(e_l, \Delta\Theta_l)$ is defined by the sum of the discounted rewards observed along one trajectory of states while following π , as follows:

$$Z^\pi(e_l, \Delta\Theta_l | \phi_l, \mathbf{y}_l, \hat{\mathcal{G}}) = \sum_{t=l}^{\infty} \gamma^{t-l} r(e_t, \Delta\Theta_t), \quad (18)$$

where $\Delta\Theta_t \sim \pi(\cdot|e_t)$, $e_{t+1} \sim P(\cdot|e_t, \Delta\Theta_t)$, and $\phi_{t+1} = \phi_t \times \Delta\Theta_t$. This cumulative discounted reward is called the *return* for each state-action pair. Next, given the current state e_l , the optimal policy that selects the best action matrix is defined to maximize such a return function, i.e.

$$\Delta\Theta_l^* = \arg \max_{\Delta\Theta} Z^\pi(e_l, \Delta\Theta). \quad (19)$$

Thus, the optimal reflection parameter for the next time slot will be $\phi_{l+1} = \phi_l \times \Delta\Theta_l^*$.

Note that, when $\gamma \approx 1$ and L is large, after multiplying by a constant duration τ , the return function in (18) approximates the objective function in (17a), and the action space \mathcal{A} is equivalent to constraint (17b). Therefore, an MDP framework properly models the optimization problem in (17). Meanwhile, an RL framework can adjust the reflection parameter ϕ_{l+1} to accommodate the actual downlink CSI and maximize the downlink rate at the end of each time slot, based on the real-time feedback \mathbf{y}_l , via (19). Thus, the IR controller does not need to measure channels for multiple times to get an accurate CSI, but use the RL model to learn the communication environment during downlink transmissions.

Unfortunately, although the aforementioned RL framework provides a suitable model, it fails to capture an essential feature of IR-aided communication system, which is the uncertainty of the reward function for each state-action pair. Note that, for each UE $k \in \mathcal{K}$, its feedback y_k has a lower rank than its downlink channel matrix \mathbf{G}_k . Thus, each signal vector \mathbf{y} corresponds to multiple channel states, and each deviation vector \mathbf{e} maps to different kinds of errors in the measured CSI $\hat{\mathbf{G}}$. In other word, even if the same action $\Delta\Theta$ is taken in the same state \mathbf{e} , different rewards can be obtained in the next time slot. Therefore, the IR-aided communication has intrinsic uncertainty on the downlink rate. Furthermore, the received noise during the information exchange phase makes the reward even less predictable, and the rate expression in (4) cannot provide an accurate estimation on the downlink rate. Therefore, it is more suitable to consider the downlink sum-rate r as a random variable, with respect to each state-action pair $(\mathbf{e}, \Delta\Theta)$, rather than a fixed number. Conventional RL frameworks, such as deep Q-learning [23], usually predict the future return by a scalar, which can be considered as the expectation of random variable r . However, in our work, we aim to account for the uncertainty of the reward function, by modeling the sum-rate r as a distribution function. Different from expectation, a return distribution provides more information on the IR-assisted transmission features, and, thus, it enables more accurate predictions on the future reward. In order to capture the randomness of downlink rate properly, the *distributional reinforcement learning* framework is introduced to model a *return distribution* for each state-action pair. Here, we stress that the distribution is not designed to capture the uncertainty in the estimation of downlink reward, but rather to model the intrinsic randomness in the MDP interaction between the IR and communication environment.

C. Distributional reinforcement learning with quantile regression

In the DRL framework [24], the return is modeled as a distribution over each state-action pair $(\mathbf{e}, \Delta\Theta)$, and the policy π maps each state $\mathbf{e} \in \mathcal{E}$ to a probability distribution over the action space \mathcal{A} . Then, the optimal policy $\pi^*(\cdot|\mathbf{e})$ that maps each state to the optimal action to maximize the expected reward can be determined by (19), which solves the optimization problem (17).

In order to model the return distribution Z , a quantile regression (QR) method is applied, which approximates the target distribution by a discrete function with variable locations of supports and fixed quantile of probabilities. Let $Z_Q = [z_1(\mathbf{e}, \phi), \dots, z_Q(\mathbf{e}, \Delta\Theta)] \in \mathcal{Z}_Q$ be the support of any Q -quantile distribution for fixed Q . Then, the Q -quantile approximation forms a discrete distribution, where $f_{Z_Q}(z_q) = \frac{1}{Q}$ for $q = 1, \dots, Q$, and the corresponding cumulative probability

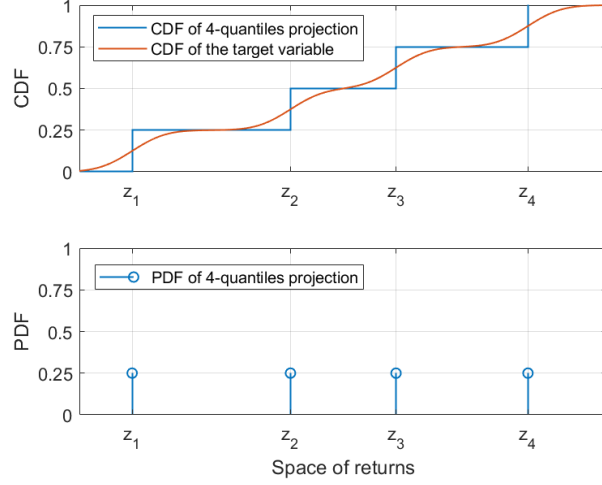


Fig. 5: An example of 1-Wasserstein minimizing projection of a target distribution Z (red line), with 4-quantiles $[z_1, z_2, z_3, z_4]$ (blue line).

is $F_{Z_Q}(z_q) = \frac{q}{Q}$. Therefore, for each state-action $(e, \Delta\Theta)$, the problem is to find the optimal values of such Z_Q that minimizes the 1-Wasserstein distance from the target Z , defined as follow,

$$d_1(Z_Q, Z) = \int_0^1 |F_{Z_Q}^{-1}(\omega) - F_Z^{-1}(\omega)| d\omega, \quad (20)$$

where F_X^{-1} is the inverse cumulative probability of distribution X . Based on Lemma 2 in [25], the optimal value of each support z_q^* that minimizes the 1-Wasserstein distance in (20) is $z_q^* = F_Z^{-1}(\frac{q+(q-1)}{2Q})$. Fig. 5 shows an example of 1-Wasserstein minimizing projection onto a 4-quantile estimation of a target distribution Z .

However, the return distribution Z of the downlink sum-rate is not explicitly known in the considered problem, and, thus, the optimal approximation result $z_q^* = F_Z^{-1}(\frac{q+(q-1)}{2Q})$ is not directly available. In order to approximate the return distribution, an empirical distribution $\hat{Z} \sim Z$ will be formed, based on the transmission feedback of e_l , Θ_l and r_{l+1} during each time slot, and \hat{Z} is used as the target distribution to model the return approximation Z_Q . In order to evaluate the approximate accuracy, we define the quantile regression loss between \hat{Z} and the Q-quantiles approximation Z_Q , for any quantile $\omega \in [0, 1]$, as [25]

$$\mathcal{L}_Z(Z_Q) = \mathbb{E}_{\hat{Z} \sim Z} \left[(\omega - \mathbb{1}_{\hat{Z} < Z_Q}) \cdot (\hat{Z} - Z_Q) \right], \quad (21)$$

where $(\omega - \mathbb{1}_{\hat{Z} < Z_Q})$ is the weight of regression loss penalty and $\hat{Z} - Z_Q$ is the deviation of Z_Q from Z . Therefore, the quantile regression loss penalizes the overestimation error with weight $1 - \omega$ and underestimation error with weight ω . However, we note that, the minimization of

convex loss function in (21) is not simply, because $\mathcal{L}_Z(Z_Q)$ is not derivable at $Z_Q = \hat{Z}$. In order to facilitate the derivation, we modify the quantile loss function, using a Huber loss, defined by:

$$\mathcal{L}_Z(Z_Q) = \mathbb{E}_{\hat{Z} \sim Z} \left[|\omega - \mathbb{1}_{\hat{Z} < Z_Q}| \cdot H(\hat{Z} - Z_Q) \right], \quad (22)$$

where $H(u) = \frac{1}{2}u^2$ for $|u| \leq \kappa$; otherwise, $H(u) = \kappa(|u| - \frac{\kappa}{2})$, where $\kappa > 0$. The modified loss function (22) is derivable everywhere. Then, the approximation problem that minimizes the quantile loss becomes

$$\min_{z_1, \dots, z_Q} \sum_{q=1}^Q \mathbb{E}_{\hat{Z} \sim Z} \left[|\omega_q - \mathbb{1}_{\hat{Z} < z_q}| \cdot H(\hat{Z} - z_q) \right], \quad (23)$$

where $\omega_q = \frac{2q-1}{2Q}$. Since the objective function is convex, we can find the minimizer $\{z_q^*\}_{q=1, \dots, Q}$ by stochastic gradient descent [22]. As a result, for each state-action pair, its return distribution $Z_Q(\mathbf{e}, \Delta\Theta)$ can be approximated by a Q-quantile $\{z_1^*(\mathbf{e}, \Delta\Theta), \dots, z_Q^*(\mathbf{e}, \Delta\Theta)\}$ via (23).

D. Optimal reflection using the DR-QRL model

In the problem of IR-aided transmissions, after observing a deviation vector \mathbf{e}_l , the IR can estimate the expected downlink rate for each action $\Delta\Theta \in \mathcal{A}$, by computing the marginal distribution of the return $Z_Q(\mathbf{e}_l, \Delta\Theta)$, via

$$V(\mathbf{e}_l, \Delta\Theta) = \mathbb{E}[Z_Q(\mathbf{e}_l, \Delta\Theta)] = \frac{1}{Q} \sum_{q=1}^Q z_q(\mathbf{e}_l, \Delta\Theta). \quad (24)$$

Here, V evaluates the summation of future transmission rates from the next time slot $l+1$ to the end of the transmission interval, if an action $\Delta\Theta$ is applied to adjust the IR coefficient, given the current signal deviation vector \mathbf{e}_l . Then, in order to maximize the sum of future data rates, the optimal reflection coefficient for the next time slot is $\phi_{l+1} = \phi_l \times \Delta\Theta^*$, where

$$\Delta\Theta^* = \arg \max_{\Delta\Theta} V(\mathbf{e}_l, \Delta\Theta). \quad (25)$$

After the IR provides downlink service to UEs using the reflection coefficient ϕ_{l+1} , the new state \mathbf{e}_{l+1} and reward r_{l+1} will be updated with the IR controller at the end of the $l+1$ time slot. The new information about the downlink transmission can be used to update the empirical distribution via a Q-learning approach, where $\hat{z}_i(\mathbf{e}_l, \Delta\Theta_l) \leftarrow r_{l+1} + \gamma z_i^l(\mathbf{e}_{l+1}, \Delta\Theta_{l+1})$, $\forall i = 1, \dots, Q$. In the end, the return distribution Z_Q^l is updated to minimize the distance from the target distribution \hat{Z} , based on (23). The training and update algorithm of the QR-DRL model for the real-time optimization of the IR reflection is summarized in Algorithm 3.

Algorithm 3 QR-DRL optimization on IR coefficient with imperfect CSI

Initialize: $0 \ll \gamma < 1$ and the DRL model $Z_Q^0 = \{z_1^0, \dots, z_Q^0\}$ for each $(e, \Delta\Theta) \in \mathcal{E} \times \mathcal{A}$.

At the beginning of a coherence interval ($l = 0$), the IR computes environment state \mathbf{y}_0 , based on the estimated CSI, and optimizes the reflection coefficient ϕ_0 , according to Algorithm 1.

For $l = 1, \dots, L - 1$, the IR controller will

1. Receive UEs' feedback \mathbf{y}_l , and compute the deviation state e_l and the reward r_l ;
2. Calculate the expected return value of the current state e_l with respect to each action $\Delta\Theta \in \mathcal{A}$ by

$$V(e_l, \Delta\Theta) = \frac{1}{Q} \sum_{i=1}^Q z_i^{l-1}(e_l, \Delta\Theta);$$
3. Adjust the reflection coefficient via $\phi_{l+1} = \phi_l \times \Delta\Theta_l$, where $\Delta\Theta_l = \arg \max_{\Delta\Theta \in \mathcal{A}} V(e_l, \Delta\Theta)$;
4. Update the empirical return distribution, using e_{l-1} , $\Delta\Theta_{l-1}$, e_l , $\Delta\Theta_l$, and r_l , via:

$$\hat{z}_i(e_{l-1}, \Delta\Theta_{l-1}) \leftarrow r_l + \gamma z_i^{l-1}(e_l, \Delta\Theta_l), \forall i = 1, \dots, Q;$$
5. Update the QR-DRL model Z_Q^l by minimizing the quantile loss between \hat{Z} and Z_Q^l via:

$$Z_Q^l = \arg \min_{\{z_q\}_{q=1, \dots, Q}} \sum_{q=1}^Q \sum_{i=1}^Q \left| \frac{2q-1}{2Q} - \mathbb{1}_{\hat{z}_i < z_q} \right| \cdot H(\hat{z}_i, z_q);$$

End

E. Convergence of the QR-DRL method

Here, we analyze the convergence property of the proposed QR-DRL approach. For any distributions Z_1, Z_2 , the maximal form of 1-Wassertein distance is defined as [24]

$$\bar{d}_1(Z_1, Z_2) = \sup_{e, \Delta\Theta} d_1(Z_1(e, \Delta\Theta), Z_2(e, \Delta\Theta)), \quad (26)$$

which will be used as the distance metric to establish the convergence of the QR-DRL method. Let Π_{W_1} be the 1-Wasserstein minimizing quantile projection, defined in (23), and \mathcal{T}^π be the distributional Bellman operator [24] that defines DRL iterations, where $\mathcal{T}^\pi Z(e, \Delta\Theta) = r(e, \Delta\Theta) + \gamma Z(e', \Delta\Theta)$. Then, the convergence of the QR-DRL projection $\Pi_{W_1} \mathcal{T}^\pi$, combined by quantile regression with the DRL operator, to a unique fixed point is given as follow.

Theorem 1. *The distance between the Q -quantile approximation Z_Q and the target return distribution Z , in terms of maximal 1-Wassertein metric, will converge to zero, via the repeated application of the QR-DRL projection $\Pi_{W_1} \mathcal{T}^\pi$, i.e. $\bar{d}_1(\Pi_{W_1} \mathcal{T}^\pi Z, \Pi_{W_1} \mathcal{T}^\pi Z_Q) \leq \gamma(\bar{d}_1(Z, Z_Q) + C_Q)$, where $\gamma \in (0, 1)$ in the discount factor in the MDP model, C_Q is a finite number that depends on the value of Q , and $\lim_{Q \rightarrow \infty} C_Q = 0$.*

Proof. See Appendix A. □

Theorem 1 shows that by applying the QR-DRL operator $\Pi_{W_1} \mathcal{T}^\pi$ once, the distance between Z and Z_Q will be changed from $\bar{d}_1(Z, Z_Q)$ to be lower than $\gamma(\bar{d}_1(Z, Z_Q) + C_Q)$. Given that $\bar{d}_1(Z, Z_Q)$ and C_Q both have finite values and $\gamma \in (0, 1)$, after the repeated application of the projection $\Pi_{W_1} \mathcal{T}^\pi$, the distance between Z and Z_Q will eventually go to zero. Therefore, the

TABLE I: Simulation and algorithm parameters

Parameters	Values	Parameters	Values
Bandwidth b	2 MHz	Number of UEs K	4
Noise power spectrum density at UE σ^2	-174 dBm/Hz	Noise power spectrum density at BS σ_{BS}^2	-170 dBm/Hz
Transmit power at BS P_{\max}	40 dBm	Transmit power at UE p_c	10 dBm
Time slot τ	0.1 s	Number of time slots per interval L	10
Uplink training subphase τ_c [13]	0.01 τ	Data transmit phase τ_d	$(1 - 0.01N)\tau$
Number of quantiles Q	40	Discount factors γ	0.9

iterative approach based on the QR-DRL projection $\Pi_{W_1} \mathcal{T}^\pi$ will converge the approximation Z_Q to the unique fixed point Z , following any policy π . Consequently, we conclude that the proposed learning approach in Algorithm 3 will converge to a unique and stable distribution of the downlink rate for the IR-aided transmission, as defined in (18), and, as a result, the optimal policy π^* that optimizes the IR coefficient ϕ can be uniquely determined, based on (24) and (25), which solves the optimal problem in (17). Therefore, the reflection optimization with limited CSI can be solved, based on to Algorithm 2 and 3, at the end of each time slot, so that the sum of future data rate is maximized from the next time slot to the end of the interval service.

V. SIMULATION RESULTS AND ANALYSIS

A. Setting

In the simulations, we consider a uniform square array of antennas at the BS with $M = 16$, and a uniform square array of IR with $N = 16$. The location of BS is fixed at $(0, 0, 25)$, the location of IR is $(0, 20, 30)$ and the location of each hotspot UE is modeled by an i.i.d. two-dimensional Gaussian $(\mathbf{x}_k, \mathbf{y}_k) \sim \mathcal{N}((0, 20), 5\mathbf{I}_2)$ with zero height. The path loss in dB is modeled [26] as $PL[dB] = 32.4 + 21 \log_{10}(d) + 20 \log_{10}(f) + \xi$, where d denotes the distance between the transmitter and receiver in meter, f is that the carrier frequency, and $\xi \sim \mathcal{CN}(0, \sigma_{sf}^2)$ denotes the small fading parameter. Given the carrier frequency $f = 30$ GHz, we set $\sigma_{sf} = 3.762$ for a LOS link, and $\sigma_{sf} = 8.092$ for a NLOS link. The MIMO channel between the BS and the IR is modeled by a rank-one matrix [27] $\mathbf{H} = \mathbf{a}^r(\varphi_0^r, \psi_0^r) \mathbf{a}^t(\varphi_0^t, \psi_0^t)^H$, where φ_0^r, ψ_0^r are the azimuth and elevation angles of arrival at IR, and φ_0^t, ψ_0^t are the azimuth and elevation angles of departure at the BS. The vectors $\mathbf{a}^r(\varphi_0^r, \psi_0^r)$ and $\mathbf{a}^t(\varphi_0^t, \psi_0^t)$ are the normalized receive/transmit array response vectors at the corresponding angles of arrival/departure, where

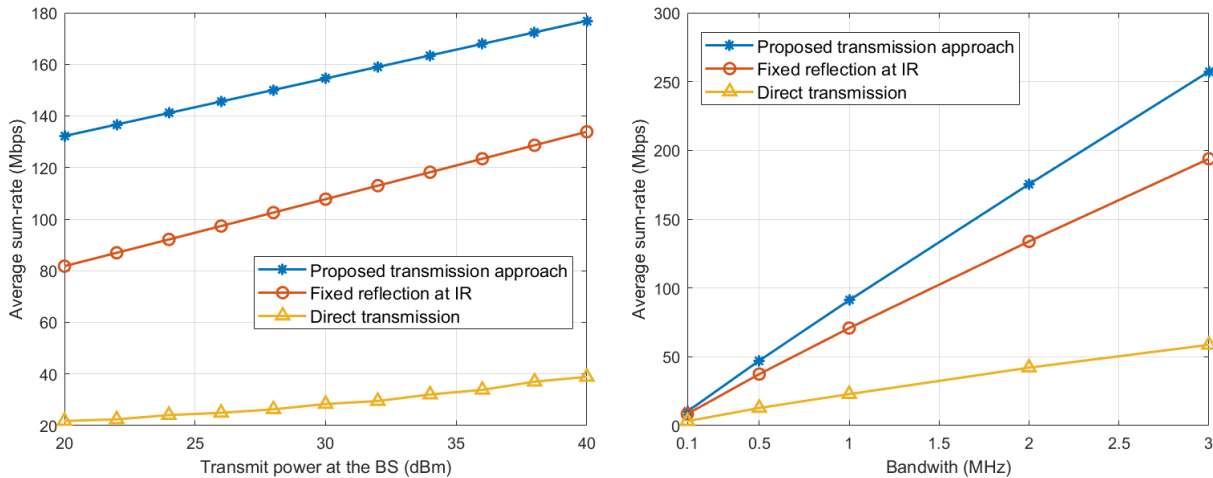
$$\mathbf{a}(\varphi, \psi) = [1, \dots, \exp(j\pi(v \sin(\varphi) \sin(\psi) + w \cos(\psi))), \dots, \exp(j\pi((V - 1) \sin(\varphi) \sin(\psi) + (W - 1) \cos(\psi)))]^T.$$

For the receiver IR, $\mathbf{a}^r(\varphi_0^r, \psi_0^r) = \mathbf{a}(\varphi_0^r, \psi_0^r)$ with $V^r = W^r = \sqrt{N}$, and for the transmitter BS, $\mathbf{a}^t(\varphi_0^t, \psi_0^t) = \mathbf{a}(\varphi_0^t, \psi_0^t)$ with $V^t = W^t = \sqrt{M}$. Similarly, the MISO channel from the IR to each UE k is modeled by a vector $\mathbf{h}_k(\varphi_k, \psi_k) = \mathbf{a}(\varphi_k, \psi_k)$ with $V_k = W_k = \sqrt{N}$, where φ_k, ψ_k are the azimuth and elevation angles of departure at the IR towards UE k . Thus, for each UE $k \in \mathcal{K}$, the MISO downlink channel is given by $\mathbf{G}_k = \frac{\exp(-j\frac{2\pi}{\lambda}d_k)}{\sqrt{PL_k}} \text{diag}(\mathbf{h}_k)\mathbf{H}$, where d_k is the distance of the connected BS-IR-UE link, and PL_k is the path loss. The values of other parameters are given in Table I.

B. IR-aided transmission with perfect CSI

In this section, we evaluate the performance of the IR-aided communication, given perfect downlink CSI. In order to show the advantage of the proposed approach, two baseline schemes are introduced, which are the direct transmission without IR reflection and the fixed IR reflection. Note that, the optimal transmission at the BS is applied in three schemes, based on to Proposition 1. However, for the direct transmission, the BS optimizes the precoding matrix and power allocation, based on the direct downlink channel. Meanwhile, after the optimization at the BS side, the fixed reflection method keeps the IR coefficient $\phi = \mathbf{I}_N$, while the proposed approach optimizes the reflection coefficient ϕ^* , based on to Algorithm 1, to further improve the downlink rate. The metric to evaluate the communication performance is the time-average downlink sum-rate within each coherence interval T . For the proposed approach, the time-average sum-rate is calculated via $(1 - \frac{N\tau_c + \tau_m}{T})r$, where $N\tau_c$ is the channel estimation time, and τ_m is for signal processing. However, for the direct transmission and the fixed IR reflection, the channel measurement is only one τ_c , and, thus, the time-average sum-rate is calculated by $(1 - \frac{\tau_c + \tau_m}{T})r$.

1) *Performance evaluation:* Fig. 6a shows that, as the BS transmit power increases from 20 to 40 dBm, the time averages of the downlink sum-rate increases in all three schemes, and the proposed method outperforms both baseline schemes. First, compared with the direct transmission without IR, the fixed reflection scheme yields 3-fold increase in downlink transmission performance, due to better channel state. Since the direct link from the BS to each UE is usually NLOS, the high path loss yields a small received power at each UE, and thus, the average downlink rate of the direct transmission is always lower than 40 Mbps. However, via a passive reflection of the IR even with a fixed coefficient, the BS-IR-UE channels can be established with LOS links, and, hence, the average rate increases significantly. Furthermore, compared with the fixed reflection scheme, our proposed method further improves the reflection coefficient after



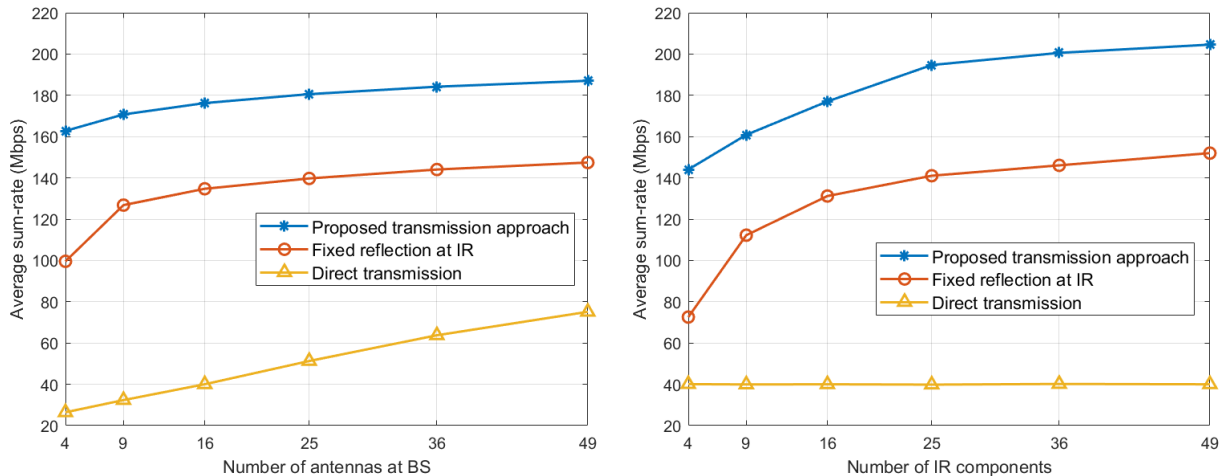
(a) The time-average downlink sum-rate increases, as the transmit power at the BS increases. (b) The time-average sum-rate increases, as the downlink bandwidth increases.

Fig. 6: The proposed approach outperforms two baseline schemes, as the transmit power and bandwidth increase.

the optimal transmission at the BS side thus achieving a performance gain of over 40 Mbps. As the transmit power of the BS increases from 20 to 40 dBm, the proposed approach yields a performance gain of 59.82% and 30.99%, compared with the fixed reflection scheme.

Fig. 6b shows that as the downlink bandwidth increases, the average downlink sum-rate of all three methods increase, and the proposed approach outperforms both baselines. Compared with the fixed reflection scheme, the achievable sum-rate of the proposed approach yields a performance gain from 21% to 33%, as the bandwidth increases from 0.1 to 3 MHz. Meanwhile, compared with the direct transmission, the proposed approach shows 2-fold increases in the downlink sum-rate. From Fig. 6, we can conclude that a large bandwidth and a higher transmit power both yield a larger achievable downlink sum-rate for the IR-aided transmission.

2) *Impact of the number of antennas:* Fig. 7 shows the relationship between the downlink sum-rate and the number of antennas at the BS and IR, respectively. First, in Fig. 7a, given that the IR has $N = 16$ reflection elements, as the number of BS antennas M increases from 4 to 49, the average sum-rate increases for all three methods, and the proposed approach yields the best performance. Given more transmit antennas, the diversity in fading multi-path channels can be achieved to improve link reliability and facilitate the zero-forcing precoding. Therefore, the average downlink rate increases for more transmit antennas at the BS. Fig. 7b shows that, given that the BS has a fixed number of antennas $M = 16$, as the number of IR reflection components increases from 4 to 49, the average sum-rate of the proposed method and the fixed reflection scheme will both increase, while the performance of direct transmission remains the same. By



(a) The time-average downlink sum-rate increases, as the number M of BS antennas increases, for $N = 16$. (b) The time-average downlink sum-rate increases, as the number N of IR components increases, for $M = 16$.

Fig. 7: The time-average downlink sum-rate increases, as the number of BS antennas or IR components increases.

deploying more reflective components at the IR, more LOS paths are created between the BS and downlink UEs, such that the received signal power at UEs will increase thus improving downlink transmission rate. Since the direct BS-UE link does not pass through the IR, the number of IR components does not impact the direct transmission scheme.

Furthermore, by comparing Figs. 7a and 7b, we can see that the average sum-rate is more sensitive to the number of IR components, than the number of antennas at the BS. Therefore, deploying more reflection components at the IR is more efficient to increase the downlink transmission rate, compared with increasing the number of BS antennas.

C. IR-aided transmission with imperfect CSI

In this section, we evaluate the performance of the IR-aided downlink transmission, given limited knowledge of CSI. Algorithm 1 is used to initialize the transmission system at the beginning of each communication interval T , and then, the proposed QR-DRL method will be applied at the end of each time slot τ , such that the distribution of downlink rate can be learned, based on the UEs' feedback, in order to improve the reflection coefficient of the IR.

1) *Preprocessing*: The DRL approach aims to model a return distribution for each state-action pair $(e, \Delta\Theta)$. Given that the state-action space is continuous, it is necessary to have a discrete $\mathcal{E} \times \mathcal{A}$, such that the number of state-action pairs, as well as the estimated distribution functions, is finitely countable. First, the state space \mathcal{E} is reduced to be a K -dimensional binary space, where for each $k = 1, \dots, K$, $e_k = 0$, if $|y_k - \hat{y}_k|^2 \leq E_{th}$; otherwise, $e_k = 1$. Here, E_{th} is a

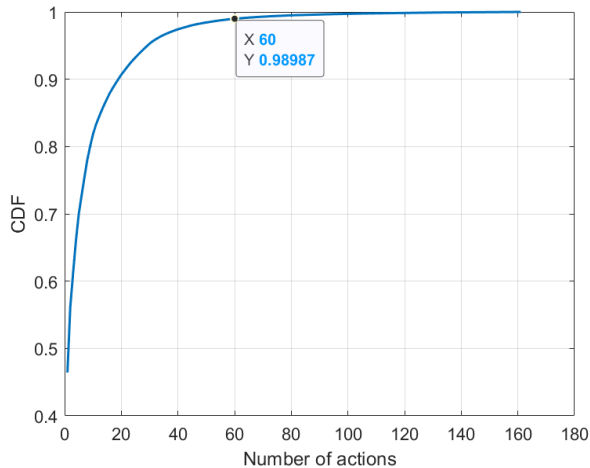


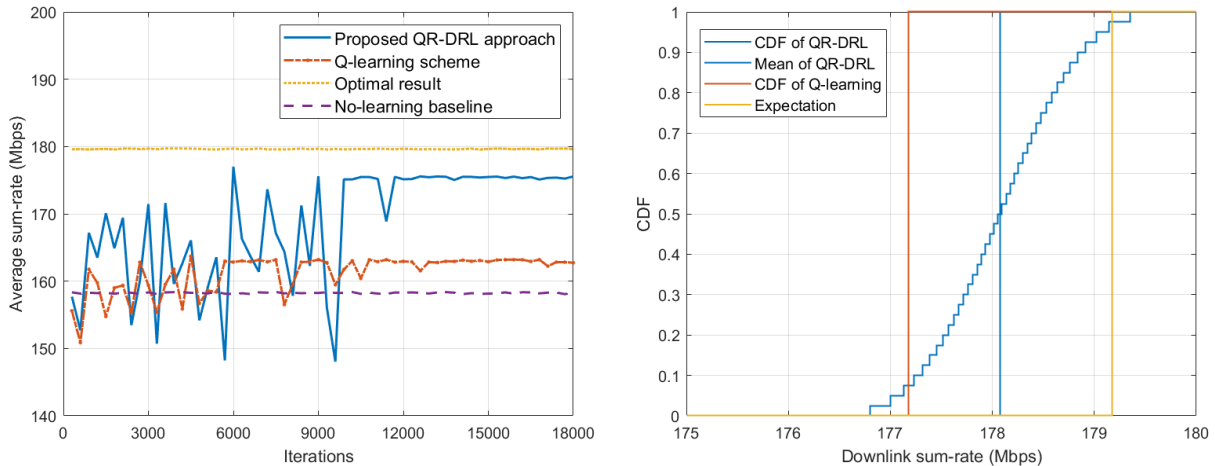
Fig. 8: A reduced set with the top 60 of the most frequent actions can cover the optimal result with an empirical probability of 99%.

threshold of the highest acceptable power for the signal deviation e . Therefore, $e_k = 0$ means that the signal deviation is small, and the downlink channel error is acceptable; otherwise, $e_k = 1$ indicates that the measured CSI \hat{G}_k of UE k is significantly different from the actual downlink CSI G_k . Consequently, the number of possible states in \mathcal{E} is 2^K . Second, in the action space \mathcal{A} , there are two possible phase change for each of the IR element n , where $\Delta\theta_n = \exp(j\pi) = -1$ means to shift the phase by π , and $\Delta\theta_n = \exp(j0) = 1$ means to keep the phase of the n -th IR component the same. Therefore, the number of possible actions in \mathcal{A} is 2^N , which increases exponentially with the number of IR components. In order to reduce the size of action space, an exhausting search algorithm is first applied to find a subsection of \mathcal{A} . As shown in Fig. 8, for a fixed number of IR components $N = 16$, we can reduce the number of actions from 2^{16} to 60, which guarantees to cover the optimal action set with a probability of around 99%.

2) *Training process*: Similar to most RL-based algorithms, the proposed QR-DRL method can be slow to converge. In order to enable an efficient reflection performance, it is necessary to train the distribution model, before the online deployment. Here, a traditional RL scheme, based on Q-learning algorithm, is introduced to compare the performance of the proposed method². Meanwhile, the result from Algorithm 1 is used as the baseline, and the optimal result, obtained based on perfect CSI, is used as the training target.

Fig. 9a illustrates the training process, in which the downlink sum-rate of the IR-aided transmission is averaged per 300 simulation episodes. First, Fig. 9a shows that the proposed

²Due to the use of neural network, deep Q-learning has a much higher computational complexity, compared with the proposed QR-DRL approach. The comparison between deep Q-learning and deep DRL methods will be subject to our future work.



(a) Training process: Average sum-rate per 300 episodes. (b) Trained distribution for state-action $(\mathbf{1}_K, \Delta\Theta_{13108})$.

Fig. 9: Average sum-rate during the training process (left) and the training result of the state-action pair $(\mathbf{1}_K, \Delta\Theta_{13108})$ (right).

QR-DRL approach converges, which supports the proof in Theorem 1. Second, compared with the Q-learning scheme, the proposed QR-DRL method has a larger variance and converges more slowly. Here, we note that the gap between the proposed learning method and the optimal result is caused by the discretion of the state-action space.

In order to provide more details on the training result, we focus on a worst-case scenario, where the deviation state $e = \mathbf{1}_K$. In this state, the received signal at each UE is significantly different from the expectation, and, therefore, the measured CSI has a large error. We compare the proposed QR-DRL approach and traditional Q-learning scheme to optimize the reflection parameter under this worst state. Fig. 9b shows the CDF of the trained return distribution for the state $e = \mathbf{1}_K$ with its optimal action No. 13108³. Fig. 9b shows that compared with Q-learning, the mean of the trained distribution from the proposed method is closer to the real expectation, which is calculated based on the error-free CSI. Instead of choosing the optimal action $\Delta\Theta_{13108}$, Q-learning is more likely to select suboptimal actions in \mathcal{A} to adjust the reflection parameters, due to its larger prediction error. Different from Q-learning that only learn the expected returns, the QR-DRL method models the return as a distribution function for each state-action pair. Compared with a deterministic expectation value, a distribution function can capture more details of the uncertainty of downlink rate, and the QR-DRL method yields a more accurate prediction than

³To convert an action $\Delta\Theta$ to its action number, first, we replace -1 by 1 and, then, we replace 1 by 0 on the diagonal of the action matrix. Second, we convert the diagonal binary vector to a decimal number and we add one. Thus, $\Delta\Theta_{13108} = \text{diag}(1, 1, -1, -1, 1, 1, -1, -1, 1, 1, -1, -1, 1, 1, -1, -1)$.

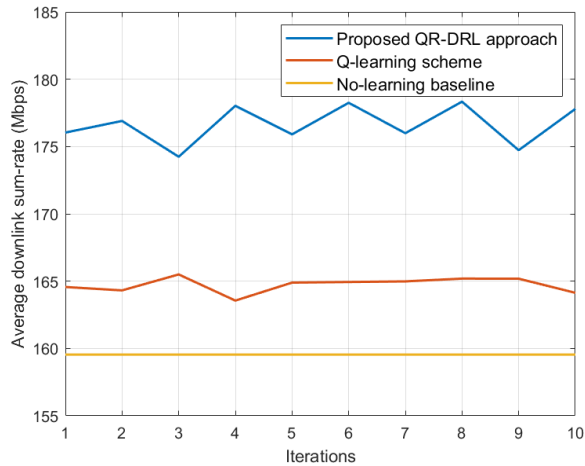


Fig. 10: Transmission performance for the online deployment.

Q-learning, for the specific state-action $(\mathbf{1}_K, \Delta\Theta_{13108})$.

3) *Performance evaluation of online deployment*: Fig. 10 shows the online performance of the proposed QR-DRL approach, with the no-learning baseline and Q-learning scheme, given imperfect downlink CSI. We run each method for 100 times and plot the average results. After an offline training stage, both the proposed QR-DRL and Q-learning models have converged. Therefore, the downlink sum-rate has a smaller variation, compared with the training phase in Fig. 9a. Meanwhile, Fig. 10 shows that the proposed QR-DRL approach improves the average data rate of the IR-aided downlink communication by around 10%, compared with the conventional RL method. Therefore, we conclude that the distribution-based prediction of the downlink sum-rate for the future time slot is more accurate, compared with a scalar-based prediction of Q-learning, and the proposed QR-DRL method enables an efficient communication of the IR-aided mmW transmission service.

VI. CONCLUSION

In this paper, we have proposed a novel framework to optimize the downlink multi-user communications of a mmW BS that is assisted by an IR. We have developed a practical approach to measure the real-time CSI. For a perfect CSI scenario, we have derived the optimal precoding transmission and power allocation to maximize the average downlink sum-rate, and, then, the IR reflection has been optimized to enhance the upper bound of the downlink capacity. Next, given imperfect CSI, we have proposed a DRL approach to learn the optimal IR reflection, so as to maximize the expectation of downlink sum-rate. In order to model the rate's probability distribution, we have developed an iterative algorithm and proved the convergence of the proposed

QR-DRL approach. Simulation results show that, given error-free CSI, the proposed transmission approach outperforms two baselines: the direct transmission scheme and a fixed IR reflection. Furthermore, under limited knowledge of CSI, simulation results show that the proposed QR-DRL method improves the average data rate by around 10% in online deployments, compared with a Q-learning baseline.

APPENDIX A

PROOF OF THEOREM 1

In order to prove that for any distribution $Z_1, Z_2 \in \mathcal{Z}$, $\bar{d}_1(\Pi_{W_1} \mathcal{T}^\pi Z_1, \Pi_{W_1} \mathcal{T}^\pi Z_2) \leq \gamma(\bar{d}_1(Z_1, Z_2) + C_Q)$, we only need to prove that, for $U = \mathcal{T}^\pi Z_1$ and $V = \mathcal{T}^\pi Z_2$,

$$\bar{d}_1(\Pi_{W_1} U, \Pi_{W_1} V) \leq \bar{d}_1(U, V) + C_Q, \quad (27)$$

where $\lim_{Q \rightarrow \infty} C_Q = 0$. Then, based on Lemma 3 in [24], we have

$$\bar{d}_1(\mathcal{T}^\pi Z_1, \mathcal{T}^\pi Z_2) \leq \gamma \bar{d}_1(Z_1, Z_2). \quad (28)$$

Combining (27) and (28), we have $\bar{d}_1[\Pi_{W_1}(\mathcal{T}^\pi Z_1), \Pi_{W_1}(\mathcal{T}^\pi Z_2)] \leq \bar{d}_1(\mathcal{T}^\pi Z_1, \mathcal{T}^\pi Z_2) + C_Q \leq \gamma(\bar{d}_1(Z_1, Z_2) + C_Q)$, which completes the proof. Next, we will focus on the proof of (27).

For notional simplification, we denote the cumulative probability function of any distribution $Z \in \mathcal{Z}$ as $F_Z(\theta) = \omega$, and the cumulative probability function of a Q-quantile estimation of Z as $F_{Z_Q}(\theta_i) = \frac{i}{Q}$, $i = 1, \dots, Q$. The p -Wasserstein distance between two distributions U and V is defined, based on (20), by

$$d_p^p(U, V) = \int_0^1 |F_U^{-1}(\omega) - F_V^{-1}(\omega)|^p d\omega. \quad (29)$$

Then, the maximal form of p -Wasserstein metric is $\bar{d}_p^p(U, V) = \sup_{\mathbf{y}, \phi} d_p^p(U(\mathbf{y}, \phi), V(\mathbf{y}, \phi))$. Without loss of generality, we assume that $\bar{d}_p^p(U, V)$ is finite. After the 1-Wasserstein minimizing projection, the p -Wasserstein distance between Q-quantile estimations $\Pi_{W_1} U$ and $\Pi_{W_1} V$ is

$$d_p^p(\Pi_{W_1} U, \Pi_{W_1} V) = \int_0^1 |F_{U_Q}^{-1}(\omega) - F_{V_Q}^{-1}(\omega)|^p d\omega = \frac{1}{Q} \sum_{i=1}^Q |F_{U_Q}^{-1}(\omega_i) - F_{V_Q}^{-1}(\omega_i)|^p, \quad (30)$$

where $\omega_i = \frac{2i-1}{2Q}$. Based on (29) and (30), we have for $p = 1$,

$$\begin{aligned} d_1(\Pi_{W_1} U, \Pi_{W_1} V) - d_1(U, V) &= \int_0^1 |F_{U_Q}^{-1}(\omega) - F_{V_Q}^{-1}(\omega)| - |F_U^{-1}(\omega) - F_V^{-1}(\omega)| d\omega \\ &\stackrel{a}{\leq} \int_0^1 |F_{U_Q}^{-1}(\omega) - F_{V_Q}^{-1}(\omega) - (F_U^{-1}(\omega) - F_V^{-1}(\omega))| d\omega \end{aligned}$$

$$\begin{aligned}
&= \int_0^1 |(F_{U_Q}^{-1}(\omega) - F_U^{-1}(\omega)) + (F_V^{-1}(\omega) - F_{V_Q}^{-1}(\omega))| d\omega \\
&\stackrel{b}{\leq} \int_0^1 |F_{U_Q}^{-1}(\omega) - F_U^{-1}(\omega)| d\omega + \int_0^1 |F_V^{-1}(\omega) - F_{V_Q}^{-1}(\omega)| d\omega = \mathcal{L}_U(U_Q) + \mathcal{L}_V(V_Q), \quad (31)
\end{aligned}$$

where $\mathcal{L}_Z(Z_Q)$ is the estimation error between distribution Z and the Q-quantile estimation Z_Q . In step (a), we have used the triangle inequality of absolute values: $|A| - |B| \leq |A - B|$, where $A = F_{U_Q}^{-1}(\omega) - F_{V_Q}^{-1}(\omega)$ and $B = F_U^{-1}(\omega) - F_V^{-1}(\omega)$, and step (b) follows from $|C + D| \leq |C| + |D|$, where $C = F_{U_Q}^{-1}(\omega) - F_U^{-1}(\omega)$ and $D = F_V^{-1}(\omega) - F_{V_Q}^{-1}(\omega)$.

The Q-quantile estimation error has an upper limit $\sup_Z \mathcal{L}_Z(Z_Q) = \frac{\bar{\theta}}{2Q}$, where $\bar{\theta}$ is the maximal value of θ . Since $\bar{d}_1(U, V) < \infty$, $\bar{\theta}$ is a finite value. Therefore, based on (31), we have

$$\sup_{\mathbf{y}, \phi} d_1((\Pi_{W_1} U(\mathbf{y}, \phi), \Pi_{W_1} V(\mathbf{y}, \phi))) \leq \sup_{\mathbf{y}, \phi} (d_1(U(\mathbf{y}, \phi), V(\mathbf{y}, \phi)) + \mathcal{L}_U(U_Q) + \mathcal{L}_V(V_Q)),$$

i.e.,

$$\bar{d}_1(\Pi_{W_1} U, \Pi_{W_1} V) \leq \bar{d}_1(U, V) + \frac{\bar{\theta}}{Q}. \quad (32)$$

By combining (32) and (28), we have $\bar{d}_1[\Pi_{W_1}(\mathcal{T}^\pi Z_1), \Pi_{W_1}(\mathcal{T}^\pi Z_2)] \leq \bar{d}_1(\mathcal{T}^\pi Z_1, \mathcal{T}^\pi Z_2) + \frac{\bar{\theta}}{Q} \leq \gamma(\bar{d}_1(Z_1, Z_2) + \frac{\bar{\theta}}{Q})$. Therefore, $C_Q = \frac{\bar{\theta}}{Q}$, and $\lim_{Q \rightarrow \infty} C_Q = \lim_{Q \rightarrow \infty} \frac{\bar{\theta}}{Q} = 0$. Consequently, let $Z_1 = Z$ and $Z_2 = Z_Q$, we have $\bar{d}_1[\Pi_{W_1}(\mathcal{T}^\pi Z), \Pi_{W_1}(\mathcal{T}^\pi Z_Q)] \leq \gamma(\bar{d}_1(Z, Z_Q) + C_Q)$.

Given that both $\bar{d}_1(Z, Z_Q)$ and C_Q have finite values and $\gamma \in (0, 1)$, a repeated application of the QR-DRL projection $\Pi_{W_1} \mathcal{T}^\pi$ will contract the distance between Z and Z_Q to zero. Therefore, the quantile approximation Z_Q will eventually converge to a unique fixed point Z .

REFERENCES

- [1] W. Saad, M. Bennis, and M. Chen, "A vision of 6G wireless systems: Applications, trends, technologies, and open research problems," *IEEE Network*, to appear, 2020.
- [2] P. Wang, Y. Li, L. Song, and B. Vucetic, "Multi-gigabit millimeter wave wireless communications for 5G: From fixed access to cellular networks," *IEEE Communications Magazine*, vol. 53, no. 1, pp. 168–178, Jan 2015.
- [3] Z. Peng, L. Li, M. Wang, Z. Zhang, Q. Liu, Y. Liu, and R. Liu, "An effective coverage scheme with passive-reflectors for urban millimeter-wave communication," *IEEE Antennas and Wireless Propagation Letters*, vol. 15, pp. 398–401, Jun 2015.
- [4] Q. Zhang, W. Saad, and M. Bennis, "Reflections in the sky: Millimeter wave communication with UAV-carried intelligent reflectors," in *Proc. of IEEE Global Communications Conference*, Hawaii, USA, Dec 2019, pp. 1–6.
- [5] C. Boyer and S. Roy, "Backscatter communication and RFID: Coding, energy, and MIMO analysis," *IEEE Transactions on Communications*, vol. 62, no. 3, pp. 770–785, Dec 2014.
- [6] X. Tan, Z. Sun, D. Koutsonikolas, and J. M. Jornet, "Enabling indoor mobile millimeter-wave networks based on smart reflect-arrays," in *Proc. of IEEE International Conference on Computer Communications*, Honolulu, HI, USA, Apr 2018, pp. 270–278.

- [7] S. Hu, F. Rusek, and O. Edfors, "Beyond massive MIMO: The potential of data transmission with large intelligent surfaces," *IEEE Transactions on Signal Processing*, vol. 66, no. 10, pp. 2746–2758, Mar 2018.
- [8] C. Huang, A. Zappone, G. C. Alexandropoulos, M. Debbah, and C. Yuen, "Reconfigurable intelligent surfaces for energy efficiency in wireless communication," *IEEE Transactions on Wireless Communications*, vol. 18, no. 8, pp. 4157–4170, Jun 2019.
- [9] Q. Wu and R. Zhang, "Intelligent reflecting surface enhanced wireless network: Joint active and passive beamforming design," in *Proc. of IEEE Global Communications Conference*, Abu Dhabi, United Arab Emirates, Dec 2018, pp. 1–6.
- [10] V. Jamali, A. M. Tulino, G. Fischer, R. Müller, and R. Schober, "Intelligent reflecting and transmitting surface aided millimeter wave massive MIMO," *arXiv preprint arXiv:1902.07670*, Sep 2019.
- [11] M. Jung, W. Saad, and G. Kong, "Performance analysis of large intelligent surfaces (LISs): Uplink spectral efficiency and pilot training," *arXiv preprint arXiv:1904.00453*, Mar 2019.
- [12] A. Taha, M. Alrabeiah, and A. Alkhateeb, "Enabling large intelligent surfaces with compressive sensing and deep learning," *arXiv preprint arXiv:1904.10136*, Apr 2019.
- [13] Q. Nadeem, A. Kammoun, A. Chaaban, M. Debbah, and M.-S. Alouini, "Intelligent reflecting surface assisted multi-user MISO communication," *arXiv preprint arXiv:1906.02360*, Jun 2019.
- [14] Y. Yang, B. Zheng, S. Zhang, and R. Zhang, "Intelligent reflecting surface meets OFDM: Protocol design and rate maximization," *arXiv preprint arXiv:1906.09956*, Jun 2019.
- [15] Q.-U.-A. Nadeem, A. Kammoun, A. Chaaban, M. Debbah, and M.-S. Alouini, "Asymptotic analysis of large intelligent surface assisted mimo communication," *arXiv preprint arXiv:1903.08127*, 2019.
- [16] S. Abeywickrama, R. Zhang, and C. Yuen, "Intelligent reflecting surface: Practical phase shift model and beamforming optimization," *arXiv preprint arXiv:1907.06002*, Jul 2019.
- [17] V. Va and R. W. Heath, "Basic relationship between channel coherence time and beamwidth in vehicular channels," in *Proc. of IEEE Vehicular Technology Conference*, Boston, MA, USA, Sep 2015, pp. 1–5.
- [18] Q. H. Spencer, A. L. Swindlehurst, and M. Haardt, "Zero-forcing methods for downlink spatial multiplexing in multiuser MIMO channels," *IEEE transactions on signal processing*, vol. 52, no. 2, pp. 461–471, Jan 2004.
- [19] M. Dai and B. Clerckx, "Multiuser millimeter wave beamforming strategies with quantized and statistical csit," *IEEE Transactions on Wireless Communications*, vol. 16, no. 11, pp. 7025–7038, 2017.
- [20] H. Guo, Y.-C. Liang, J. Chen, and E. G. Larsson, "Weighted sum-rate optimization for intelligent reflecting surface enhanced wireless networks," *arXiv preprint arXiv:1905.07920*, 2019.
- [21] K. Shen and W. Yu, "Fractional programming for communication systems—part I: Power control and beamforming," *IEEE Transactions on Signal Processing*, vol. 66, no. 10, pp. 2616–2630, Mar 2018.
- [22] S. Wright and J. Nocedal, "Numerical optimization," *Springer Science*, vol. 35, no. 67-68, p. 7, 1999.
- [23] V. Mnih, K. Kavukcuoglu, D. Silver, A. Graves, I. Antonoglou, D. Wierstra, and M. Riedmiller, "Playing atari with deep reinforcement learning," *arXiv preprint arXiv:1312.5602*, 2013.
- [24] M. G. Bellemare, W. Dabney, and R. Munos, "A distributional perspective on reinforcement learning," in *Proceedings of the 34th International Conference on Machine Learning-Volume 70*. JMLR. org, 2017, pp. 449–458.
- [25] W. Dabney, M. Rowland, M. G. Bellemare, and R. Munos, "Distributional reinforcement learning with quantile regression," in *Thirty-Second AAAI Conference on Artificial Intelligence*, 2018.
- [26] "5G channel model for bands up to 100 GHz," Oct. 2016, [Online]. Available: <http://www.5gworkshops.com/5GCM.html>.
- [27] O. El Ayach, R. W. Heath, S. Abu-Surra, S. Rajagopal, and Z. Pi, "The capacity optimality of beam steering in large millimeter wave mimo systems," in *IEEE International Workshop on Signal Processing Advances in Wireless Communications*, Cesme, Turkey, June 2012.